Table 1 Critical values

	$w=0$		$P=0$			
α	$\frac{P_o a^2}{EI}$	$\frac{v_c}{a}$	$\frac{w_o a^3}{EI}$	$\frac{W_o a^2}{EI}$	$\frac{v_c}{a}$	$\frac{P_o}{W_o}$
30°	22.65	0.0327	35.72	37.41	0.00110	0.606
40°	17.15	0.0597	19.85	27.72	0.00350	0.619
50°	13.82	0.0953	12.42	21.67	0.00825	0.638
60°	11.44	0.1353	8.225	17.23	0.01614	0.664
70°	9.462	0.1711	5.574	13.62	0.0268	0.695
80°	7.617	0.1921	3.755	10.49	0.0385	0.726
90°	5.861	0.1946	2.498	7.846	0.0495	0.747
100°	4.287	0.1828	1.607	5.611	0.0573	0.764
110°	2.975	0.1607	0.999	3.835	0.0609	0.776
120°	1.944	0.1334	0.596	2.495	0.0601	0.779
135°	0.886	0.0882	0.248	1.169	0.0508	0.758

from the origin; the curve for $\alpha = 60°$ is in part convex and in part concave; and the remaining curves are slightly concave. Only one of the interaction curves ($\alpha = 80°$) is presented in this Note, Fig. 1, in order to illustrate the degree of curvature. The determination of the character of an interaction curve (stability boundary) is often a significant problem,[7] for, if the curve is convex away from the origin (away from the region of stability), the straight-line approximation, Eq. (1), yields critical load values which are on the safe side.

Equation (1) together with Table 1 will enable the designer rapidly and accurately to estimate the critical (buckling) loads for two-hinged circular arches. With these data we observe that the (modified) critical point load P is obtained by subtracting from P_o the values $(P_oW/W_o) =$ from $0.61W$ to $0.78W$ for arches with $\alpha = 30°$ to $120°$. Lind's suggested values[8] of $(P_oW/W_o) =$ from $0.50W$ to $0.67W$ are good for arches shallower than $\alpha = 60°$. It is interesting to note that the values of (P_oW/W_o) increase with increasing α up to about $\alpha = 120°$ and then start decreasing.

Now let us make use of the calculated results to re-examine the experimental data in Ref. 9. The total weight W of a semi-circular arch specimen of radius $a = 10$ in. was 0.255 lb or, since $EI/a^2 = 0.677$ lb, $W = 0.377EI/a^2$. Substitution of this value in Eq. (1), in which, according to Table 1, $P_o = 5.86EI/a^2$, yields $P = 5.58EI/a^2$ or 3.78 lb. The experimental plot of the point load vs the horizontal crown displacement[9] deviates from the load axis at $P = 3.7$ lb, a discrepancy of less than 3%.

References

[1] Lo, C. F. and Conway, H. D., "The Elastic Stability of Curved Beams," *International Journal of Mechanical Sciences*, Vol. 9, No. 8, Aug. 1967, pp. 527–538.

[2] Conway, H. D. and Lo, C. F., "Further Studies on the Elastic Stability of Curved Beams," *International Journal of Mechanical Sciences*, Vol. 9, No. 10, Oct. 1967, pp. 707–718.

[3] Schmidt, R. and DaDeppo, D. A., "Large Deflections of Eccentrically Loaded Arches," *Zeitschrift für angewandte Mathematik und Physik*, Vol. 21, No. 6, 1970, pp. 991–1004.

[4] DaDeppo, D. A. and Schmidt, R., "Large Deflections of Elastic Arches and Beams with Shear Deformation," *Industrial Mathematics*, Vol. 22, Pt. 1, 1972, pp. 17–34.

[5] Huddleston, J. V., "Finite Deflections and Snap-Through of High Circular Arches," *Journal of Applied Mechanics*, Vol. 35, No. 4, Dec. 1968, pp. 763–769.

[6] DaDeppo, D. A. and Schmidt, R., "Stability of Heavy Circular Arches with Hinged Ends," *AIAA Journal*, Vol. 9, No. 6, June 1971, pp. 1200–1201.

[7] Huseyin, K., "The Elastic Stability of Structural Systems with Independent Loading Parameters," *International Journal of Solids and Structures*, Vol. 6, 1970, pp. 677–691.

[8] Lind, N. C., "Elastic Buckling of Symmetrical Arches," TR 3, 1962, Univ. of Illinois Engineering Experiment Station, Urbana, Ill.

[9] Langhaar, H. L., Boresi, A. P., and Carver, D. R., "Energy Theory of Buckling of Circular Elastic Rings and Arches," *Proceedings of the Second U.S. National Congress of Applied Mechanics*, June 1954, pp. 437–443.

Time-Asymptotic Solution for Sphere-Cones in Hypersonic Flow

PRABHAKARA P. RAO* AND JAMES M. LEFFERDO†

Martin Marietta Aerospace Corp., Denver, Colo.

Introduction

CURRENTLY, spherically-blunted cones are receiving prime attention as planetary entry configurations since such shapes have favorable ballistic coefficients, ability to tailor convective and radiative environments and efficient internal packaging characteristics. Several different approaches to solve these blunt body problems are currently available in computer program form. For small angled spherically-blunted cones, the inverse method combined with the method of characteristics has been successfully applied.[1] The method of integral relations[2] or its combination with the method of characteristics[3] has been used for either large or small cone angles. However, these methods cannot provide solutions to the blunt body problem over an intermediate range of cone angles where mixed supersonic-subsonic flow occurs on the conical portion of the body.

The purpose of this Note is to demonstrate the applicability of the time-asymptotic method to a full range of cone angles. This method can treat mixed subsonic and supersonic regions because of its technique of transforming the flow equations into hyperbolic form. Furthermore, it provides detailed flowfield properties including sonic line location and encounters no difficulty throughout the complete range of body geometry. The ensuing analysis is based on the computer solution of Barnwell[4] which is modified to treat the body surface and sonic corner more accurately.

Analysis

The fluid dynamic equations for an inviscid flow of a perfect gas in the shock layer can be cast in the divergence form using a body-oriented coordinate system as

$$(\partial F/\partial t)+(\partial P/\partial x)+(\partial Q/\partial y)+R=0 \tag{1}$$

where

$$F=\lambda r\begin{vmatrix}\rho\\ \rho u\\ \rho v\\ \rho E\end{vmatrix},\quad P=r\begin{vmatrix}\rho u\\ p+\rho u^2\\ \rho uv\\ \rho uH\end{vmatrix},\quad Q=\lambda r\begin{vmatrix}\rho v\\ \rho vu\\ p+\rho v^2\\ \rho vH\end{vmatrix},$$

$$R=\begin{vmatrix}0\\ -p\lambda\cos\Theta+Kr\rho uv\\ -p\lambda\sin\Theta-Kr(p+\rho u^2)\\ 0\end{vmatrix} \tag{2}$$

The boundary conditions behind the shock are specified by the Rankine-Hugoniot relations for a moving shock with its velocity determined by a characteristic compatability relation.

In order to obtain an accurate distribution of surface flow variables, the boundary conditions should reflect a true description of the flow at the surface. Therefore, instead of using the flow equations directly as adopted by Barnwell,[4] the surface flow properties are determined using the unsteady characteristic compatability relations which represent more accurately the physical aspects of the flow on the surface. Furthermore, the

Received June 22, 1973; revision received October 4, 1973. This work was supported under the Martin Marietta Aerospace Independent Research and Development Program, and was accomplished while the senior author was working in the Planetary Physics Section.

Index categories: Supersonic and Hypersonic Flow; Shock Waves and Detonations.

* Senior Engineer, System Performance Analysis Section. Member AIAA.

† Head, Gas Physics Unit. Member AIAA.

sonic conditions at the body corner are specified explicitly in lieu of approximate flow equations in the modified form.[4]

Equation (1) is solved numerically using an explicit two-step finite-difference method of Brailovskaya, which has the form

$$F^*(t+\Delta t,x,y) = F(t,x,y)+(\partial F/\partial t)\Delta t \quad (3)$$

$$F(t+\Delta t,x,y) = F(t,x,y)+(\partial F^*/\partial t)\Delta t \pm \phi_x \pm \phi_y \quad (4)$$

where ϕ_x and ϕ_y are the damping terms,[4] which are determined by invoking the Von Neumann condition in a linear stability analysis.

Since the body shapes of interest include curvature discontinuity points where large flow variable gradients can occur, a dissipative finite-difference scheme is adopted to suppress possible short-wave oscillations of the flow properties and avoid the necessity of using a fine mesh spacing at the junction regions. Furthermore, the scheme is stabilized in the vicinity of junction points and the sonic corner by locally augmenting the dissipation.

Results and Discussion

In order to demonstrate the applicability of the time-asymptotic method to treat body shapes for which the inverse and integral methods or their combination with the method of characteristics are unsuitable, sphere-cone shapes with cone half angles ranging from 40° to 70° are considered. These body shapes are similar to those considered in Ref. 5. The freestream conditions correspond to a Mach number of 47.5 and a constant specific heat ratio of 1.27. Numerical computations were carried out on a CDC 6500 computer with a typical run-time of about 6.5 min to obtain a converged solution for a 55° sphere-cone shape with 21 points on the surface and 7 strips in the shock layer.

The salient features and significant changes in the flowfield surrounding the sphere-cone blunt bodies are illustrated in Fig. 1. The supersonic flow on the conical part of low angle bodies changes completely into subsonic flow at higher angles. At small cone angles the surface pressure on the conical part has a ten-

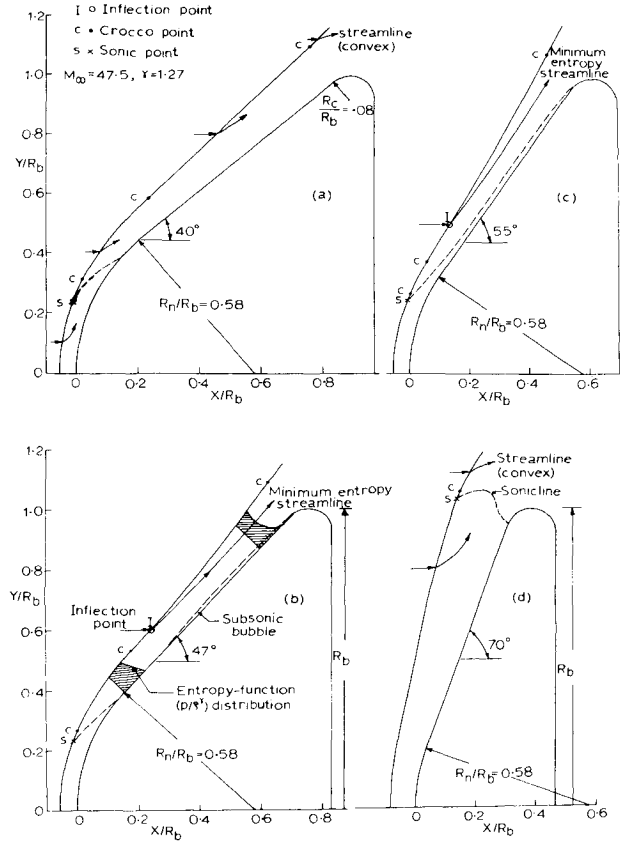

Fig. 1 Shock shapes for various sphere-cones.

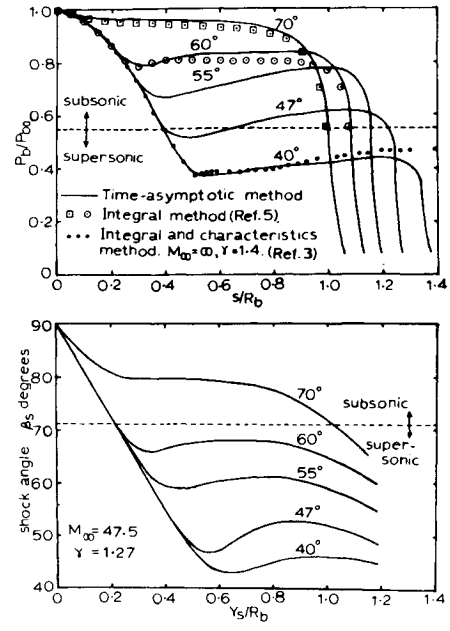

Fig. 2 Pressure distribution and shock angle for various sphere-cones.

dency to approach asymptotically that of a sharp cone. However, the surface Mach number will attain a value considerably lower than its conical flow value. When the cone half angle is in the vicinity of about 47°, a "subsonic bubble" appears on the aft portion of the body resulting in three sonic points on the surface. In such cases, inadequacy of the integral method to account for more than one sonic point[6] on the surface restrains its applicability. Also, the presence of subsonic flow on the surface prevents the use of the method of characteristics. The subsonic bubble spreads rapidly with cone angle by an upstream movement of the intermediate sonic point, and finally the sonic points at the sphere-cone junction region disappear resulting in a complete subsonic flow on the surface.

Contrary to the results observed for highly blunted bodies, more than one Crocco point (the point where streamline curvature is zero) will be located on the shock for small cone angles. These points on the shock indicate the locations where the streamlines behind the shock change their shape. Further discussion concerning the Crocco point and its significance will be found in Ref. 7. With an increase in cone angle, the distance between two Crocco points adjacent to the junction decreases and finally these points disappear at large cone angles. Beyond the sphere-cone junction, an inflection point appears on the shock due to its concavity, which is attributed to the interaction of the bow shock with the compression waves emanated during the rapid pressure recovery at the junction. For increased cone angles, the inflection point moves closer to the junction leading to a smaller entropy layer and hence a larger entropy gradient at the aft end of the body. In order to account properly for the increased entropy gradient effects, several strips are necessary to ensure that a sufficient number of points lie within the entropy layer.

The surface pressure distribution on various sphere-cone bodies with cone half angles ranging from 40° to 70° is shown in Fig. 2. The computational results compare favorably with those of the method of integral relations for both 60° and 70° sphere-cones[5] for which the flow on the surface is completely subsonic. Moreover, the present results of a 40° sphere-cone, for which the flow on the conical part is completely supersonic, compare well with the results of Ref. 3, which uses the Belotserkovskii's integral relations method[2] on the spherical part and the method of characteristics on the conical part. It is evident that the flow changes from supersonic to subsonic on the conical part for cone half-angles in the vicinity of 47°. Although the region of

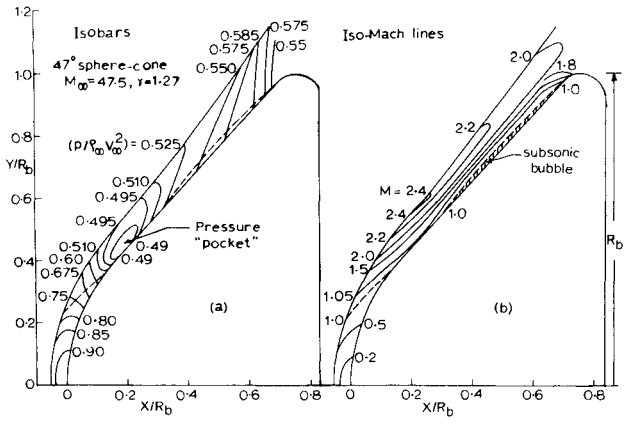

Fig. 3 Isobars and iso-Mach lines for a 47° half-angle sphere-cone.

adverse pressure gradient monotonically decreases with cone angle, its magnitude will attain a maximum value for cone angles in the vicinity of 47°.

Figure 2 also presents the variation of shock angle with radial distance from the axis. The shock shape up to the sonic point is unaffected until the cone angle is close to the detachment angle of a sharp cone. The location of the shock sonic point rapidly changes with further increase in the cone angle. The concavity of the shock in the sphere-cone junction region reveals the possibility of having three shock sonic points for certain cone angles between 60° and 70° to include a small region of supersonic flow in the vicinity of the inflection point.

Interesting observations will be made from the contours of isobars and iso-Mach lines in the shock layer of a 47° sphere-cone. Figure 3 depicts the presence of a pressure "pocket" near the surface, which is attributed to the proximity of the inflection point to the sphere-cone junction. This pressure pocket disappears at both small and large cone angles. The iso-Mach lines in the spherical portion of the body exhibit a monotonic decrease of Mach number from the shock to body surface. However, the Mach number in the conical portion increases to a maximum value and then decreases as the body surface is approached.

The present results demonstrate the capability of the time-asymptotic method, with proper accounting for the entropy layer, to treat a wide range of sphere-cone bodies. In addition, the supersonic flow on the conical part of a small angle body changes into subsonic flow at large angles with the appearance and spreading of a subsonic bubble on the surface at intermediate cone angles. This pronounced change in the flow characteristics significantly modifies the shock wave and sonic line shapes, and results in the appearance of a pressure pocket and an adverse pressure gradient at the junction region.

References

[1] Inouye, M., Rakich, J. V., and Lomax, H., "A Description of Numerical Methods and Computer Programs for Two-Dimensional and Axisymmetric Supersonic Flow Over Blunt-nosed and Flared Bodies," TN-D-2970, Aug. 1965, NASA.

[2] Belotserkovskii, O. M., ed., "Supersonic Gas Flow Around Blunt Bodies," TT-F-453, June 1967, NASA.

[3] Chushkin, P. I. and Shulishnina, N. P., "Tables of Supersonic Flow About Blunted Cones," Computation Center Monograph, Academy of Sciences, Moscow, USSR, 1961, translated and edited by J. F. Springfield, RAD-TM-62-63, 1962, AVCO Corp., Greenwich, Conn.

[4] Barnwell, R. W., "A Time-Dependent Method for Calculating Supersonic Angle-of-Attack Flow About Axisymmetric Blunt Bodies with Sharp Shoulders and Smooth Nonaxisymmetric Blunt Bodies," TN-D-6283, Aug. 1971, NASA.

[5] Edquist, C. T., "Aeroheating of Sphere Cones and Spherical Segment Probes During Venus Entry," TN-P73-203434-061, Feb. 1973, Martin Marietta Aerospace Corp., Denver, Colo.

[6] Traugott, S. C., "Some Features of Supersonic and Hypersonic Flow About Blunted Cones," *Journal of the Aerospace Sciences*, Vol. 23, No. 4, April 1962, pp. 389–399.

[7] Rao, P. P., "Streamline Curvature and Velocity Gradient Behind Curved Shocks," *AIAA Journal*, Vol. 11, No. 9, Sept. 1973, pp. 1352–1354.

Large Amplitude Forced Vibrations of Elastic Structures

L. W. REHFIELD*
Georgia Institute of Technology, Atlanta, Ga.

Introduction

AEROSPACE vehicle structures are largely composed of thin-walled elements stiffened by beam-like members or made of composite construction. These elements are often caused to vibrate at large amplitudes during certain phases of flight. Consequently, large amplitude vibrations are of considerable interest and a number of papers have been written on the subject. An extensive bibliography of recent papers published on large amplitude flexural vibrations of thin elastic plates and shells has been compiled by Pandalai.[1]

A general approach to nonlinear free vibrations of elastic structures has been developed by the present author.[2,3] The approach is based upon Hamilton's principle and a perturbation procedure and is in much the same spirit as Koiter's theory of initial postbuckling behavior.[4,5] It provides information regarding the first-order effects of finite displacements upon the frequency and dynamic stresses arising in free, undamped vibration of structures.

In the present Note the general approach just described is extended to the technically important case of forced vibrations. The structure is assumed to be excited by a disturbing force which is a harmonic function of time and is spatially distributed so as to drive only a single mode. The theory reduces to that of free vibrations in the absence of a disturbing force. Also, linearized vibration theory is recovered for small amplitude motion. Applications to the forced, undamped vibrations of beams and rectangular plates are presented as illustrations.

Basic Equations

The functional notation of Budiansky[6] will be utilized to permit a concise presentation of the theory. The applied loading q produces generalized displacement u, strain γ, and stress σ. The dynamics of the system is established by Hamilton's principle, which, for periodic motion with circular frequency ω, can be symbolically written[7]

$$\int_0^{2\pi} [\omega^2 M(\ddot{u}) \cdot \delta u + \sigma \cdot \delta\gamma - q \cdot \delta u]\, d\tau = 0 \qquad (1)$$

The "dot" operation signifies the appropriate inner multiplication of variables and integration of the result over the entire structure. The generalized mass operator M is assumed to be homogeneous and linear with the property that

$$M(u) \cdot v = M(v) \cdot u \qquad (2)$$

for all u and v. $\tau = \omega t$ is the time variable, t is time and $(\dot{}) = \partial(\ )/\partial\tau$. δu is any virtual displacement that is consistent with the kinematic boundary conditions imposed on the structure.

Received July 27, 1973. This work was supported by the United States Air Force Office of Scientific Research under Grant AFOSR-73-2479.

Index category: Dynamic Structural Analysis.

* Associate Professor of Aerospace Engineering. Member AIAA.